Nucleosome Reconstruction via Phosphorus Mapping

George Harauz and F. P. Ottensmeyer

Summary. Electron spectroscopic imaging was combined with reconstruction algorithms to derive the three-dimensional structure of the nucleosome core particle to a resolution of 1.5 nanometers. Images of phosphorus distributions within individual nucleosomes were interpreted as projections of a supercoil of DNA. These were used to orient the corresponding individual nucleosome images, making it possible to reconstruct the entire nucleosome in three dimensions. The structure is consistent with known biochemical and biophysical data and explains site-specific nuclease sensitivity, although differing in part with other nucleosome models.

The predominant approach to determination of the three-dimensional structure of a macromolecule or complex has been x-ray crystallography. However, the difficulty of obtaining large and sufficiently perfect crystals increases as macromolecules and complexes increase in size. As a result, alternative techniques are being developed that depend on the use of the electron microscope, a device that yields information from extremely small, more easily obtained crystals or even from individual particles.

Electron micrographs of one-dimensional repeating structures such as helical viruses or polypeptides, and two-dimensional macromolecular crystals imaged at different known relative angles, have been used to compute three-dimensional structures (*1*), while images of individual molecules, if sufficiently simple, have been interpreted directly in three dimensions (*2*). A computer reconstruction technique, akin to tomographic reconstruction used today in medical x-ray imaging (*3*), can be applied to electron micrographs of more complex individual structures if different views of the same structure at known relative angles can be obtained (*4*). The latter is a formidable task, since a series of views of a single object at different known tilt angles can seldom be acquired, because of the sensitivity of biological specimens to electron bombardment. In principle, a single image of a number of separate, identical particles is sufficient, provided that the relative orientations of the particles can be determined (*5, 6*).

We have been able to derive the orientation of individual nucleosome cores by a new technique, electron spectroscopic imaging, which permits not only normal electron microscopy of the structure but also the direct visualization of the DNA component within each nucleosomal particle. This component image is so great a structural simplification that an iteratively refined model of the path of DNA within the nucleosome was sufficient to establish the relative angles. When these angles were used, the total nucleosomal DNA-protein complex was reconstructed to a resolution of about 1.5 nm.

George Harauz is a graduate student in the Department of Medical Biophysics, University of Toronto. F. P. Ottensmeyer is a professor in the Department of Medical Biophysics, University of Toronto, and research physicist at the Ontario Cancer Institute, 500 Sherbourne Street, Toronto, Ontario, Canada M4X 1K9.

Direct Three-dimensional Reconstruction

Electron micrographs of nucleosomes can be considered projections at different angles of a single nucleosome particle (Fig. 1). Knowledge of the angles which relate the projections to the three-dimensional particle can be used to convert the individual electron micrographs, suitably filtered, into a three-dimensional volume in which the original structure is reconstructed. The orientation of each random projection of the nucleosome is determined by comparing the path of DNA within each nucleosome with a simulated model projected at different specified angles to give a corresponding view.

The Nucleosome

The nucleosome core is a particulate complex comprising 146 base pairs (bp) of DNA and two copies each of four histone proteins (H2A, H2B, H3, and H4) (*7*). Although the main role of the nucleosome appears to be compaction of DNA, processes such as transcription and replication must also be interpreted in view of the structure of the nucleosome.

Many biochemical and biophysical techniques have been used to probe parts of the nucleosome structure directly or inferentially, most notably x-ray diffraction of chromatin fibers and nucleosome crystals (*8, 9*), electron microscopy of tubular aggregates of the histone octamer (*10*), neutron scattering to obtain an average measure of the relative location of DNA and protein (*11*), nuclease digestion kinetics to probe the accessibility or exposure of the DNA (*12*), and chemical cross-linking studies to place the histone proteins relative to each other and to the DNA molecule (*13*). Based on these data, a fairly detailed model of nucleosome structure has been proposed in which the eight histone proteins form a compact, wedge-shaped core about which the DNA is wound. The path of the 2-nm thick DNA strand is a left-handed superhelix of 1.8 turns with an outer diameter of 10.8 nm and a pitch of 2.8 nm. The entire nucleosome is approximately 11 nm in diameter and 5.5-nm high, with the density roughly divided into two equal halves about a dyad axis of symmetry.

The proposed path of DNA in the nucleosome, which has been described as a supercoil on the outside of the particle, is central to this model of nucleosome structure. The radii of gyration of the nucleic acid and protein components, derived from neutron scattering studies of nucleosomes in solution, are crucial to the construction of the model (*11*). These radii, which are effectively mathematical condensations of the structures into equivalent spherical or ellipsoidal shells, permit numerous models which must then be constrained by other data such as contiguity of the DNA molecule or outside dimension of the particle. One advantage of electron microscopy is that it produces a directly interpretable image. Moreover, the development of electron spectroscopic imaging (*14*) allows the direct visualization of the DNA component in the nucleoprotein complex, and the determination of its relationship to the protein component with a potential resolution of about 0.5 nm (*15, 16*).

Electron Spectroscopic Imaging

Electron spectroscopic imaging is a technique that combines electron microscopy with electron energy loss analysis. Electrons incident upon a specimen interact with it in a number of different ways, including (i) elastic collisions and (ii) inelastic interactions that give rise to excitation and ionization of valence and inner shell atomic electrons. For ionization of inner shell atomic electrons, the incident electron loses an amount of energy that is characteristic of the atomic element. An imaging spectrometer installed in our transmission electron microscope disperses electrons that have interacted with the specimen into a spectrum of energy losses, and via a slit system selects electrons within a narrow band of energy losses with which a high resolution image is formed. Elemental maps can be obtained from such high resolution images which delineate specific atom distributions with a sensitivity of detection of about 50 atoms (*16*).

Since phosphorus is a constituent primarily of nucleic acid and not of protein, images of the spatial distribution of phosphorus within a nucleoprotein complex are effectively images of the nucleic acid component. Phosphorus maps are obtained from a pair of electron spectroscopic images taken at energy losses of 150 and 110 electron volts (eV), which bracket the phosphorus $L_{2,3}$ ionization threshold at 132 eV (*14, 15*). The 110-eV image contains general structural information including that on protein and DNA. The 150-eV image contains, in addition, an enhanced phosphorus signal. The difference between the images after suitable normalization is the net phosphorus distribution, while either image or the sum of both provides information on the total structure.

This approach has been used to examine nucleosomes in chromatin (*16, 17*), isolated ribosomal subunits (*18*), thinly sectioned crystals of ribosomal subunits, and ribonucleoprotein complexes. In this article, it is used specifically to derive the relative orientation of individual nucleosome particles.

Specimen Preparation and Electron Microscopy

To provide the necessary self-consistent set of images of identical nucleosomes, core particles were isolated from calf thymus by the method of Lutter (*12*) with slight modifications. Good yields of nucleosome cores were obtained with a narrow range of sizes of DNA around 146 bp (Fig. 2) and a full complement of the four core histones in approximately equimolar amounts, as determined by gel electrophoresis (*19*). In order to minimize drying artifacts, the nucleosome cores were fixed in glutaraldehyde before being applied to the grid, and processed by critical point drying (*20*).

Pairs of electron spectroscopic images of high optical quality were selected that bracketed the phosphorus ionization energy and were digitized with picture elements of size 0.53 by 0.53 nm (Fig. 3a). Digital nucleosome images were then examined individually. Images of dimers, aggregates, and subnucleosomal particles were rejected on the basis of integral optical density. Other images were rejected if the nucleosomes appeared distorted or severely altered by electron bombardment. This procedure left 100 nucleosome particles out of 227 digitized images for which the phosphorus distribution was analyzed in detail to determine the relative orientation. The average signal-to-noise ratio of the phosphorus signal over regions of individual nucleosomes was 52.4 ± 10.1, confirming the reality of the signal. To ensure a 1.0-nm spatial resolution within an 11.0-nm diameter region in a reconstruction from noise-free images, only 15 uniformly distributed orientations are required (*6*). The final reconstruction was carried out with 55 nucleosome images.

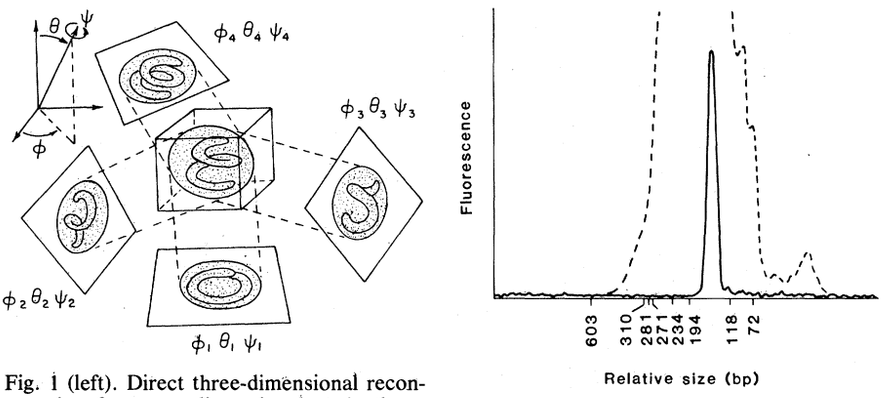

Fig. 1 (left). Direct three-dimensional reconstruction from two-dimensional projections. The two-dimensional images are projections of a representative nucleosome viewed at orientations described by three angles (φ, θ, and ψ). An estimate of the original three-dimensional density distribution can be reconstructed by computationally projecting suitably filtered images back into the three-dimensional volume. Fig. 2 (right). Densitometer scans across photographs of ethidium bromide–stained polyacrylamide gels of DNA extracted from the nucleosome core preparation. Hae III restriction fragments of φX174 were used as molecular weight markers. The solid line indicates a lane with 2 μg of DNA showing the predominant 146-bp length corresponding to nucleosome cores. The dotted line indicates an adjacent lane overloaded with 35 μg of DNA, showing a consistent band at 40 to 45 bp.

Orientation Determination

A digital model of a supercoil representing the path of nucleosomal DNA was computed from which projections could be generated at any specified orientation. The orientation of an image of nucleosomal phosphorus was determined initially by visual comparison with a gallery of these model projections at 10-degree intervals, and subsequently refined interactively on the computer until a reasonable match was found. A purely computational approach was assessed to be prohibitively slow. Methods such as multivariate analysis could assist this process but have not been sufficiently developed, particularly for three dimensions (*5*).

After the images had been aligned, a three-dimensional reconstruction was made with the use of a direct filtered back-projection algorithm (*6*). Projections of the reconstruction were correlated by computer with individual phosphorus images. The orientation of the phosphorus images was refined by means of a self-consistency seeking algorithm (*6*), and a new reconstruction was made. Through several cycles of the alignment and reconstruction process, the simulated DNA model was refined as well, in order to achieve greater consistency with the nucleosomal phosphorus distribution. An example of a comparison of a phosphorus distribution with the model at a final set of angles is shown in Fig. 3b (*21*). The distribution of projection directions of all phosphorus images used is shown in Fig. 3c. While some anisotropy is observed, possibly due to preferred orientations on the specimen support, virtually all orientations of the nucleosome are represented.

Initially, a simulated supercoil of unit density, outer diameter 10.8 nm, pitch 2.7 nm, width 2.0 nm, and 1.8 turns was

generated (Fig. 4, model 1). This represents the current model for the path of nucleosomal DNA. Since it is not possible to determine handedness from our projections, a left-handed supercoil was used throughout. Comparison with phosphorus maps of individual nucleosomes revealed that under our experimental conditions, the images of the phosphorus distribution differed consistently from the initial model. Consequently, our simulated DNA model was refined by altering both the pitch and diameter of the supercoil, yet retaining the fixed length of DNA required by biochemical analysis. The final conformation of the DNA distribution that was most consistent with the phosphorus maps was a supercoil with an outer diameter of 8.5 nm, pitch 4.0 nm, width 2.0 nm, and 2.4 turns comprising 146 bp of DNA (Fig. 4, model 2). During this process, the reconstructions consistently indicated an additional strong phosphorus signal distinct from the supercoil and located at a short distance from the presumptive dyad axis. This unexpected phosphorus signal was incorporated into the final model (Fig. 4, model 3), and the alignment and reconstruction performed again.

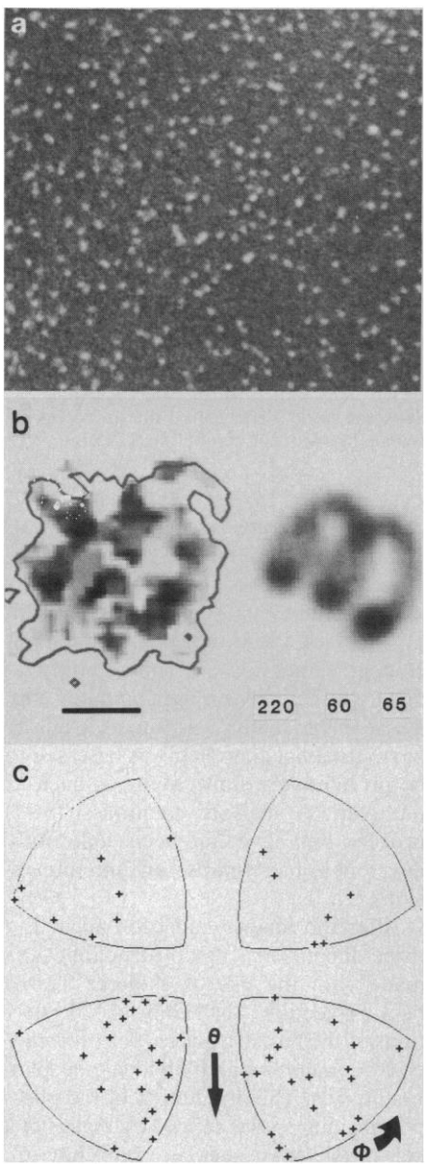

Fig. 3. (a) Electron spectroscopic image of unstained, critical point dried nucleosome cores. The image was formed with electrons that had lost 150 eV of energy ± a window size of 6 eV. The total dose was about 1.4 coulombs per square centimeter. Magnification, ×41,700. (b) The phosphorus distribution of a single nucleosome core with the outline of the total particle (left). The projection of a supercoil model (right) at the corresponding orientation defined by three angles (ϕ, θ, ψ). The scale bar represents 5 nm. (c) The distribution of orientations of a population of 55 randomly oriented nucleosomes represented as crosses on a unit hemisphere which is viewed from above. The four quadrants of the hemisphere have been separated and "lifted." The top of the hemisphere corresponds to the point (ϕ, θ) = (0, 0). The value of θ increases along lines of longitude (straight arrow). Along lines of latitude, θ is constant but ϕ changes (curved arrow). The third angle, ψ, represents a rotation of the image plane and is not shown.

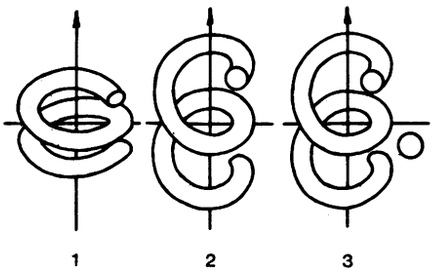

Fig. 4. Model supercoils representing the path of nucleosomal DNA. Supercoil 1 is a current published model (*7, 10*). Model 2 shows an alteration in pitch and radius indicated by present results. Model 3 incorporates an extra phosphorus signal distinct from the supercoil. A dyad axis in the coil runs from left to right.

The Phosphorus Structure

The first step in the reconstruction of the entire nucleosome is the calculation of the three-dimensional distribution of the phosphorus signal representing the DNA in the particle (Fig. 5a). A control reconstruction (Fig. 5b) using model 3 and the same set of angles as the phosphorus images (Fig. 3c), in comparison with the model itself (Fig. 5c) shows no discernible artifacts arising from the limited number and partly anisotropic distribution of projection directions. Common structural features in the reconstructions of the phosphorus distribution and of the model (Fig. 5, a and b) are the open circle in the view along the helix axis, the zig-zag in the two orthogonal side views, and the additional unanticipated phosphorus signal. Relative to the integrated phosphorus signal of the DNA (292 phosphorus atoms), this additional signal comprises about 30 to 40 phosphorus atoms. A hexagonal shape is seen when the reconstructed phosphorus structure is viewed along the supercoil axis. In a wooden model, this shape was due to substantial kinks in the DNA (*22*) separated by slightly bent segments either 10 bp or 20 bp in length.

The difference in conformation between the three-dimensional phosphorus reconstruction and model 1 can have a number of explanations. One likely possibility is that, in spite of prior glutaraldehyde fixation, the process of dehydration in preparation for critical point drying altered the conformation of the protein core and expanded the helix torsionally along the supercoil axis to conserve the length of DNA. This would be in agreement with the 3.8- and 8.0-nm x-ray periodicities observed upon drying of chromatin fibers (*8*). However, the core particle also alters its conformation in response to changes in ionic strength, hydrophobicity, *p*H, concentration, and even upon removal of histone H1 during its isolation (*7, 23*), and has apparently a quite different shape in its active form (*17, 24*). The elongated conformation observed may be one of a number of relevant naturally occurring configurations. Uniformity in shape of individual particles must nevertheless be assumed, since the reconstruction would otherwise be excessively blurred. The phosphorus reconstruction agrees with the 4.9-nm radius of gyration measured from neutron scattering (*11*), and the total reconstruction (below) can be interpreted easily in terms of known results on histone-DNA cross-linking (*13*) and on sensitivity to nuclease digestion (*25*).

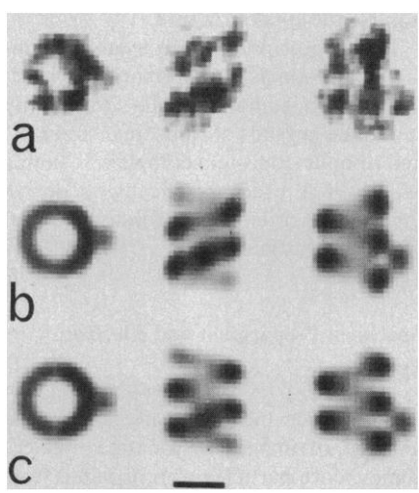

Fig. 5. Orthogonal views of (a) the reconstruction of nucleosomal phosphorus computed from 55 images and (b) the reconstruction computed from the same orientations of model 3. (c) The original model 3. The scale bar represents 5 nm.

Nucleosomal Protein Structure

The original electron spectroscopic images of the nucleosomes (Fig. 3a) from which the orientation of the DNA supercoil was derived contain information concerning both protein and DNA in the core particle. By means of the same sets of angles as were used for the corresponding phosphorus distribution, these nucleosome images were used to reconstruct the total three-dimensional structure. The 150-eV and 110-eV images were reconstructed separately. However, since they contained the same protein information except for random differences, they have been summed here to provide a three-dimensional structure with a better signal-to-noise ratio than either set of images separately. The regions in the total reconstruction that contain the previously determined phosphorus distribution were then set to zero to produce a structure containing protein information only. The hydrated volume of the histone octamer of 137 nm^3 (*10, 26*) served as a guide in defining the boundaries of the protein reconstruction from which a balsa wood model was built (Fig. 6). The contour cutoff used in constructing the model was somewhat lower than indicated by the hydrated volume in order to preserve contiguity of the structure.

The entire nucleosome has the shape of a prolate ellipsoid approximately 10 nm in length and about 9 nm in diameter. The protein component forms a spool with discontinuous protrusions forming a helical ridge of about two turns. The DNA rests between the protein ridges, albeit with a fair portion of the supercoil exposed on the surface. In addition, smaller protein densities envelope the DNA partially or completely at symmetrically placed points (Fig. 6). These may be the basic lysine- and arginine-rich amino terminal domains of the core histones. There is a major central cavity within the protein core, and other minor solvent channels result in a porous octamer complex. The extra phosphorus signal is held to the particle by a small amount of protein to form an asymmetrical protrusion or "bustle."

Dyad Symmetry

One of the central features of the model 1 nucleosome core particle is the existence of a dyad axis of symmetry, inferred from both nuclease digestion kinetics studies of isolated nucleosomes (*12*) and reconstruction from electron micrographs of helical arrays of the protein octamer (*10*). In the present study, the asymmetry of the extra phosphorus signal in the DNA model permitted both a potential symmetrical or unsymmetrical structure of the histone component in the reconstruction. Nevertheless, twofold symmetry was observed not only in the major internal protein densities but also in minor extensions between the DNA loops and outside them (Fig. 6). The rotational cross-correlation coefficient was highest at 180 degrees for the core region exclusive of the asymmetrical bustle. Its calculated value of 0.41 was not as high as had been expected from a visual impression of the symmetry of the model. The deviation from perfect symmetry must be due to a lack of high frequency correlation, distortion between the two halves, random differences, and a nonuniform distribution of orientations (Fig. 3c). However, the value is similar to other experimentally observed correlation coefficients of three-dimensional reconstructions at similar resolution (*4*).

The extra phosphorus signal provided a reconstruction unbiased by imposed symmetry. The presence of this signal, however, is puzzling. A specific retrospective search by polyacrylamide gel electrophoresis for smaller nucleic acid fragments extracted from the nucleosome core preparation revealed a fainter but consistent band migrating at a position equivalent to 40 to 45 bp (Fig. 2) which on preliminary examination was sensitive to alkaline conditions. The relationship of this band to the extra phosphorus signal is currently under investigation.

Histone Localization

The spatial resolution of the protein reconstruction was limited by the digitization of the images to 1.06 nm. This resolution is not limited by the data, as the measured signal-to-noise ratio over individual nucleosomes in the sum of the two-dimensional spectroscopic images was 5.1 ± 1.1 per picture element, indicating that the images could have been digitized even more finely (*27*). However, errors in the assignment of angles for the reconstruction could decrease the spatial resolution to 1.5 nm. This resolution is not sufficient to distinguish between the various histones. Nevertheless, one can assign probable positions to the histones using the chemical cross-linking data of Mirzabekov and colleagues (*13, 28*) (Fig. 7) and the assumption that less dense regions in the computed protein structure represent boundaries between individual histones. Thus,

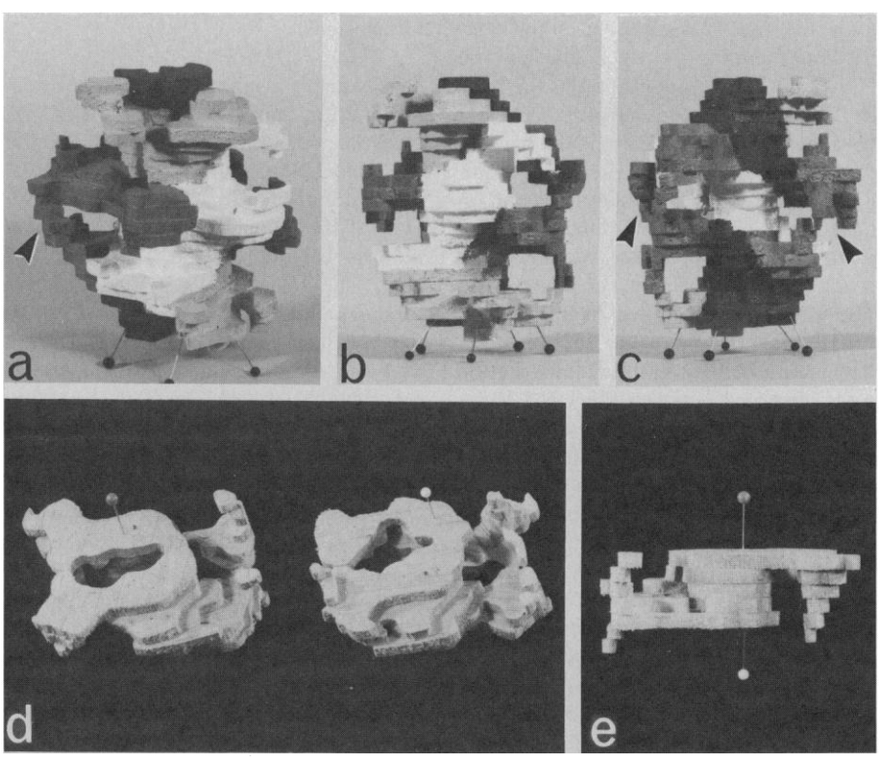

Fig. 6. A balsa wood model of the reconstructed nucleosomal protein component. (a) An oblique and slightly skewed side view. The dyad axis of symmetry runs from the left background to the right foreground; (b) and (c) are front and back views, respectively. Shades of gray delineate interpretations of histone positions. (d) Two faces of the midsection of the protein component. (e) A back view of the midsection in (d). In (d) and (e), dark and light pins are used to distinguish the two faces. Dyad symmetry and a central cavity are evident.

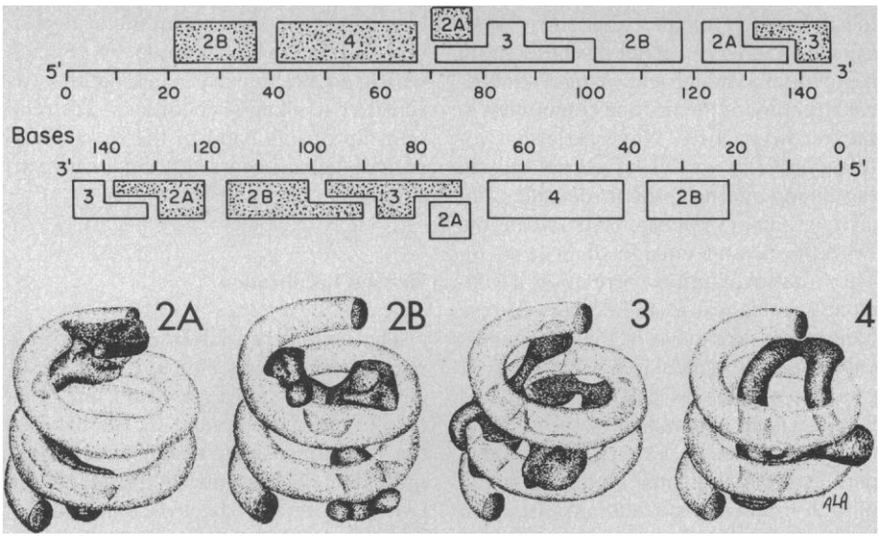

Fig. 7. (Top) Schematic summary of histone-DNA cross-linking data [redrawn from (*27*)]. (Bottom) Interpretations of the configurations of histones H2A, H2B, H3, and H4, based on cross-linking data (*13, 28*) and the three-dimensional reconstruction. The orientations shown correspond to those in Fig. 6a.

histones H2A and H2B have been positioned at the extreme top and bottom of the complex. Histone H2A has been shown to cross-link to two noncontiguous sites on the DNA at 70 to 80 bases and 120 to 130 bases from the 5′ end. In our altered supercoil, with about 60 bp per turn (model 3), these sites are almost superposed. Histone H3 cross-links to both the central and end portions of the DNA supercoil, and thus the two H3 molecules are placed along either side, partly extending between the central DNA loops and reaching across the back to lie underneath the ends of the DNA. Histones H4 are placed along the front of the nucleosome, reaching diagonally inward towards the top and bottom and on to the back. The H3-H4 tetramer therefore can be interpreted as two interdigitating U-shapes forming a central cavity. These interpretations are diagrammed in Fig. 7.

Protein densities in the reconstruction were observed between the DNA loops as well as at specific points outside them. The nucleosome core remains particulate after mild trypsinization, which removes the amino terminal ends of the histones from the nucleosome core, indicating that these domains are not essential to nucleosome structure (*25, 29*). Whitlock and Simpson (*25*) have shown that the rate of deoxyribonuclease I digestion of some susceptible sites located 20 to 35 bp and 60 to 80 bp from the 5′ DNA termini increases after mild trypsinization of the nucleosome cores, indicating that the amino terminal domains of some histones interact with these regions of the nucleosomal DNA. Examination of our reconstruction revealed that protein densities were closely associated with the DNA at positions 20 and 35 and virtually surrounded the DNA in the regions 60 and 80 bp from the ends. Thus, the structure offers a natural explanation for such specific changes in digestion sensitivity.

Conclusions

The net phosphorus and net protein distributions of critical point dried nucleosome cores have been reconstructed in three dimensions directly from two-dimensional electron spectroscopic images of individual nucleosomes lying in random orientations on a carbon support. The results suggest that this approach can be used to study noncrystallized nucleosomes in various forms, such as transcriptionally active nucleosomes (*17, 24*), chromatosomes (*30*), and subnucleosomes (*31*), as long as a homogeneous population can be obtained. It should be possible to examine other nucleoprotein complexes such as ribosomal subunits (*18*), ribonucleoprotein particles, and transcriptional complexes with electron spectroscopic imaging. The spatial resolution limit has not been reached in our studies. Resolution can be improved with the use of a greater number of projections, a more uniform distribution of orientations, and additional techniques such as cryopreservation of the specimen (*32*) and, where possible, crystallization (*33*).

References and Notes

1. R. A. Crowther and A. Klug, *Annu. Rev. Biochem.* **44**, 161 (1975); S. D. Fuller, *Methods Cell Biol.* **22**, 251 (1981); G. Harauz, D. W. Andrews, F. P. Ottensmeyer, *Ultramicroscopy* **12**, 59 (1983).
2. F. P. Ottensmeyer, R. F. Whiting, A. P. Korn, *Proc. Natl. Acad. Sci. U.S.A.* **72**, 4953 (1975); A. M. Fiskin, D. V. Cohn, G. S. Peterson, *J. Biol. Chem.* **252**, 8261 (1977); A. P. Korn and F. P. Ottensmeyer, *J. Theor. Biol.* **105**, 403 (1983).
3. R. Gordon and G. T. Herman, *Int. Rev. Cytol.* **38**, 111 (1974).
4. V. Knauer, R. Hegerl, W. Hoppe, *J. Mol. Biol.* **163**, 409 (1983); H. Oettl, R. Hegerl, W. Hoppe, *ibid.*, p. 431.
5. J. Frank, *Methods Cell Biol.* **22**, 325 (1981); M. van Heel, in *Proceedings of the 41st Annual Meeting of the Electron Microscopy Society of America*, G. W. Bailey, Ed. (San Francisco Press, San Francisco, 1983), p. 460; A. Verschoor, J. Frank, M. Radermacher, T. Wagenknecht, M. Boublik, in *ibid.*, p. 758.
6. G. Harauz and F. P. Ottensmeyer, *Ultramicroscopy* **12**, 309 (1984).
7. J. D. McGhee and G. Felsenfeld, *Annu. Rev. Biochem.* **49**, 1115 (1980).
8. M. H. F. Wilkins, G. Zubay, H. R. Wilson, *J. Mol. Biol.* **1**, 179 (1959); J. A. Subirana, F. Azorin, J. Roca, J. Lloveras, R. Llopis, J. Cortadas, in *The Molecular Biology of the Mammalian Genetic Apparatus*, P. O. P. Ts'o, Ed. (North-Holland, Amsterdam, 1977), vol. 1, pp. 71–92.
9. J. T. Finch *et al.*, *Nature (London)* **269**, 29 (1977).
10. A. Klug, D. Rhodes, J. Smith, J. T. Finch, J. O. Thomas, *ibid.* **287**, 509 (1980).
11. R. P. Hjelm *et al.*, *Cell* **10**, 139 (1977).
12. L. C. Lutter, *J. Mol. Biol.* **124**, 391 (1978).
13. V. V. Shick, A. V. Belyavsky, S. G. Bavykin, A. D. Mirzabekov, *ibid.* **139**, 491 (1980); H. G. Martinson, R. True, C. K. Lau, M. Mehrabian, *Biochemistry* **18**, 1075 (1979).
14. F. P. Ottensmeyer and J. W. Andrew, *J. Ultrastruct. Res.* **72**, 336 (1980).
15. K. M. Adamson-Sharpe and F. P. Ottensmeyer, *J. Microsc. (Oxford)* **122**, 309 (1981).
16. D. P. Bazett-Jones and F. P. Ottensmeyer, *Science* **211**, 169 (1981).
17. ———, *Can. J. Biochem.* **60**, 364 (1982).
18. A. P. Korn, P. Spitnik-Elson, D. Elson, F. P. Ottensmeyer, *Eur. J. Cell Biol.* **31**, 334 (1983).
19. R. L. Rill, B. R. Shaw, K. E. van Holde, *Methods Cell Biol.* **18**, 69 (1978).
20. T. F. Anderson, *Trans. N.Y. Acad. Sci.* **13**, 130 (1951).
21. G. Harauz and F. P. Ottensmeyer, an extensive gallery of such comparisons is part of a manuscript in preparation.
22. F. H. C. Crick and A. Klug, *Nature (London)* **255**, 530 (1975); H. M. Sobell, C.-C. Tsai, S. G. Gilbert, S. C. Jain, T. D. Sakore, *Proc. Natl. Acad. Sci. U.S.A.* **73**, 3068 (1976).
23. R. E. Harrington, *Biochemistry* **21**, 1177 (1982); N. V. Beaudette, H. Okabayashi, G. D. Fasman, *ibid.*, p. 1765; E. C. Uberbacher, V. Ramakrishnan, D. E. Olins, G. J. Bunick, *ibid.* **22**, 4916 (1983).
24. C. P. Prior, C. R. Cantor, E. M. Johnson, V. C. Littau, V. G. Allfrey, *Cell* **34**, 1033 (1983).
25. J. P. Whitlock and R. T. Simpson, *J. Biol. Chem.* **252**, 6516 (1977).
26. B. W. Matthews, *J. Mol. Biol.* **33**, 491 (1968).
27. A. Rose, *Vision: Human and Electronic* (Plenum, New York, 1973), p. 14.
28. A. D. Mirzabekov, *Trends Biochem. Sci.* **6**, 240 (1981).
29. D. M. J. Lilley and K. Tatchell, *Nucleic Acids Res.* **4**, 2039 (1977); J. P. Whitlock and A. Stein, *J. Biol. Chem.* **253**, 3857 (1978).
30. R. T. Simpson, *Biochemistry* **17**, 5524 (1978).
31. D. A. Nelson, A. J. Mencke, S. A. Chambers, D. K. Oosterhof, R. L. Rill, *ibid.* **21**, 4350 (1982).
32. M. K. Lamvik, D. A. Kopf, J. D. Robertson, *Nature (London)* **301**, 332 (1983).
33. N. Unwin and R. Henderson, *Sci. Am.* **250** (No. 2), 78 (1984).

34. Supported by the Medical Research Council of Canada, the National Cancer Institute of Canada, the Ontario Cancer Treatment and Research Foundation, and a Medical Research Council Studentship (G.H.). We thank Dr. P. N. Lewis for biochemical advice, Elizabeth Macpherson for preparative help and biochemical follow-up, Dr. Larry Arsenault for drawing the protein configurations in Fig. 7, and the David Dunlap Observatory of the University of Toronto for use of the flat-bed densitometer.